Post-stack iterative modeling migration and inversion (IMMI)

Gary F. Margrave

SUMMARY

The possibility of a post-stack process resembling full-waveform inversion (FWI) is investigated. As generalized by the IMMI concept, this implies an iterative process of modeling, migration, and inversion all done in the post-stack domain. To test this idea, a detailed stratigraphic p-wave velocity model was created by interpolating between 3 sonic logs from the Hussar dataset. The overburden (upper 200m) was created with smooth lateral and vertical gradients, and the underburden (1.55km to 2km depth) has similar smooth gradients while the detailed stratigraphy is contained in the 200m-1.55km interval. The wells were placed at 1km, 2km, and 3km distances along the line, the interpolation was guided by picked formation tops, and the resulting velocity model was created on a 2.5m square grid (2D). Using acoustic finite-difference modeling, 60 shot records were created at even intervals along the 4km line. The data were then processed with gain, f-k filter, normal-moveout removal, and stack to create a conventional CMP stack. Then, an IMMI process of exploding reflector modeling, post-stack migration, and matching to known impedance at a presumed well was employed. The exploding reflector modeling was chosen for its simplicity compared to the modeling and processing of all 60 shots in each iteration. The migration was a post stack depth migration, and the matching to well control was conducted using a single simulated well at coordinate 1000m. It was assumed that the overburden (upper 200m) velocity was known through tomography or refraction statics and it was further assumed that the velocity was known in detail at the well from 200m to 1.55km depth. The starting model contained the true overburden and then a simple linear gradient from the base of the overburden to a presumed-known basement velocity of 4500m/s. Shown below is the result after 11 iterations during which the maximum frequency allowed into the process was gradually increased from 10 to 60 Hz. At each step in the iteration, the depth migration at the well was scaled to approximately match the well velocity and this scaling was then applied to the entire migration. While a better result is desired, the process appears to be both feasible and worthwhile.

INTRODUCTION AND BACKGROUND

Recent experience with FWI (full-waveform inversion) has shown that it can be generalized to a process called *iterative modelling, migration, and inversion* or IMMI. Both FWI and IMMI are designed to estimate an earth model from seismic data and both involve an iteration loop that produces progressively refined models. Additionally, they both require a starting model that is smooth and 'close' to the true model. Using the starting model, the iteration loop starts by predicting synthetic data that is compared to the real seismic data. The data residual, meaning the subtraction of the synthetic data from the real data, is then migrated which associates the data residual with subsurface locations. The processes differ in the nature of the migration algorithm that is used. FWI theory (e.g. Tarantola 1984, Pratt 1999, Virieux and Operto 2009, and others) indicates that a particular formulation of RTM (reverse-time migration) is preferred. Unlike migration in data processing, this formulation estimates a model perturbation (typically

impedance or, if density is assumed constant, velocity) and makes no overt correction for wavefront spreading. In contrast, a data processing migration estimates reflectivity (roughly the derivative of a model perturbation) and always compensates for wavefront spreading. The migrated data residual is called the *gradient* in FWI parlance because it arises as the gradient of the objective function which is the sum of squares (L_2 norm squared) of the data residual. Therefore, it follows that the objective function can be decreased by stepping the direction opposite to the gradient, however the size of the step is not immediately prescribed. In other words, the gradient needs to be scaled by a value called the step length and then added to the starting model to predict the model to be used in the next iteration. This description is called a steepest descent algorithm and often requires a great many iterations. The slow convergence is often attributed to the poor scaling of the gradient (i.e. the lack of wavefront spreading corrections mentioned previously, see Shin et al, 2001) and methods exist to improve this called Newton or Gauss-Newton methods. In theory, the gradient needs a correction operator called the *inverse Hessian* to account for the poor scaling and a Newton method uses the exact inverse Hessian while a Gauss-Newton method uses an approximation. These methods should converge in fewer steps than steepest descent but not necessarily in less time because the inverse Hessian is notoriously difficult to compute.

In contrast to FWI, IMMI proposes to use a standard industry depth migration to migrate the data residual thus estimating a reflectivity perturbation. The conversion of reflectivity to impedance (or velocity) is a familiar process in data processing and known as matching-to-wells plus *impedance inversion*. IMMI suggests that the model update be calculated according to common practice when well logs are available for matching. The potential advantages here are strong. Using any well-crafted migration allows the use of tools that have been tweaked and polished over many years. Moreover, while RTM has its advantages, other migration approaches such as depth-stepping often produce sharper results in less time. Since industry migration codes always incorporate wavefront spreading corrections, gradient estimates using these codes should be comparable to FWI using an approximate inverse Hessian and hence should converge more rapidly.

Confining our attention to steepest descent methods, following the estimation of the gradient by migration of the data residual, the estimation of the step length is the final problem in an iteration. Assuming for the moment that the gradient represents a velocity perturbation (i.e. constant density) and not reflectivity, in FWI the step length is a scalar, a, such that the objective function decreases meaning

$$\sum_{s,g}[\psi(s,r) - \psi_{n+1}(s,r)]^2 = \varphi_{n+1} < \varphi_n, \qquad (1)$$

where $\psi(s,r)$ is the real recorded data for source s and receiver r, $\psi_{n+1}(s,r)$ is the estimated synthetic data from velocity model $v_{n+1}(x,y,z)$, and φ_n is the objective function for velocity model $v_n(x,y,z)$. Furthermore, it is assumed that

$$v_{n+1}(x,y,z) = v_n(x,y,z) + aG_n(x,y,z), \qquad (2)$$

where $G_n(x,y,z)$ is the n^{th} gradient estimate. So, a is a number such that when used to scale the gradient and added to the current velocity model a better velocity model is produced in the sense that the predicted data better matches the real data. Thus the

velocity model is validated by matching the data and so this is called *data validation*. In a typical FWI, the actual value of the step length a is found by a so-called line search. This is a 1-D search over possible values of a where for each tested value a trial updated velocity model is created, used to predict synthetic data, and a new objective function is computed. At least 3 values of a must be tested, one too large, one too small, and one near the expected optimum. The optimum is then estimated by quadratic interpolation.

While not rejecting data validation, IMMI proposes an alternative validation at well control (Margrave et al, 2012). Called well validation, the step length a is chosen such that

$$\sum_z [v_w(z) - v_n(x_w, y_w, z) - aG_n(x_w, y_w, z)]^2 = min, \tag{3}$$

where $v_w(z)$ is the observed velocity in the well, x_w, y_w are the map coordinates of the well (assumed vertical), and the sum is take over all depths where velocity was measured in the well. An explicit solution for the step length is

$$a = \frac{\sum_z \delta v(z) G_n(z)}{\sum_z G_n^2(z)}, \tag{4}$$

where $\delta v(z) = v_w(z) - v_n(x_w, y_w, z)$. This expression assumes that the gradient estimates a velocity perturbation not reflectivity. Since most industry migrations estimate reflectivity, a relationship between velocity and reflectivity at constant density is

$$r_k = \frac{v_{k+1} - v_k}{v_{k+1} + v_k} \sim \frac{\Delta v_k}{2v_k}, \tag{5}$$

where the subscript k denotes a subsurface layer, r_k is the reflection coefficient between layers k and $k+1$, and in the second expression $\Delta v_k = v_{k+1} - v_k$ and $v_{k+1} + v_k \sim 2v_k$. Now, assume something similar to equation 5 applies at the n^{th}iteration and write

$$\Delta v_n = 2v_n r_n \tag{6}$$

where r_n is now the reflectivity estimate produced by migrating the data residual, v_n is the migration velocity model, and then Δv_n is the predicted update to the velocity model. Of course, we must allow for the migrated data residual to require at least an undetermined scalar to approximate a reflection coefficient, and we determine this scalar at a well. So, in direct analogy to equation 3, we pose the least-squares problem

$$\sum_z [v_w(z) - v_n(x_w, y_w, z) - 2aG_n(x_w, y_w, z) v_n(x_w, y_w, z)]^2 = min. \tag{7}$$

Thus the updated velocity model will be $v_{n+1} = v_n(1 + 2aG_n)$ whereas in equation 3 it was $v_{n+1} = v_n + aG_n$. If the migration method used is calibrated to estimate reflectivity as most are, then equation 7 should be better suited. The analytic solution to equation 7 is

$$a = \frac{\sum_z \delta v(z) v_n(z) G_n(z)}{2\sum_z v_n^2(z) G_n^2(z)}. \tag{8}$$

So there are two alternative methods of estimating the step length. Equation 1, when solved using a line search, is the usual method in FWI and is referred to as data validation because the optimal a is chosen to minimize the sum-squared data residual. The

alternative well validation is proposed by IMMI and is essentially routinely practised in modern data processing. In well validation, the estimated reflectivity, a.k.a. the migrated data residual, is matched to that observed in wells and then converted to velocity (or impedance). The suggestion made here of finding a multiplicative scalar is perhaps the simplest possible form of matching to a well, and there are many more possible adjustments including phase rotation, gain adjustment, match filtering, wavelet estimation and deconvolution, dynamic time warping, and more. Most of these methods are routinely used in industry and most are time-domain methods while the gradient is typically estimated in depth. Thus a depth to time conversion may be useful for optimal matching.

It is very likely that methods using both data validation and well validation will prove superior. The two forms of validation have different properties and sensitivities and these can be exploited.

A major difficulty with both FWI and IMMI is the computational burden involved. Each iteration involves both a data simulation (forward modelling) and a depth migration. For a modern seismic dataset containing many thousands of source gathers, even a single iteration can be computationally formidable and typical FWI experiences involve tens or hundreds of iterations. Therefore, ideas that might reduce the number of iterations or the cost of any iteration are of great interest. IMMI using well validation can reduce the number of iterations dramatically. In this paper, the possibility of reducing the per-iteration effort is investigated by examining a post-stack implementation of IMMI. This can reduce cost in several ways. First, a post-stack depth migration is much less computation than the corresponding prestack process. Second, the process of CMP (common midpoint) stacking with all of the associated machinery is designed to suppress wavetypes like Rayleigh waves and shear waves that require elastic physics and fine spatial sampling to model or migrate. Third, it is possible to simulate a CMP stacked section directly without first modelling the individual source records thereby greatly reducing the simulation effort. The most obvious way to do this is to exploit the exploding reflector concept (Loewenthal et al, 1977). This paper investigates this possibility.

The next section describes the synthetic data constructed for this test. This data is acoustic constant-density finite difference created using a velocity model created from spatially interpolated well logs and therefore containing much stratigraphic detail. After simulation, the created shot records were processed and stacked. Using a finite-difference implementation of the exploding reflector model, an exploding reflector section is also simulated and compared to the CMP stack and to a theoretical seismogram at a simulated well. Then the post-stack IMMI process is discussed and results are shown for several different frequency-dependent iterations.

THE SYNTHETIC DATASET

If FWI or IMMI are to become practical processes, then perhaps the most appropriate setting would be a stratigraphic play with minimal structural complexity. With this in mind, a stratigraphic dataset was simulated using well logs available from the Hussar project (Margrave et al, 2011). Figure 1 shows a log section that was spatially

interpolated from three wells at Hussar (14-35, 14-27, and 12-27) which all have very long sonic logs available. The three well logs all start near 200m depth and extend to about 1550m depth. The spatial positions of the wells are chosen for convenience and do not represent their actual positions along the Hussar line. Formation tops (there are more than shown in the figure) guided the interpolation so that thicking or thinning formations resulted in stretched or squeezed logs. Between two wells, interpolated logs are an inverse distance weighted combination of samples from the two wells. The logs shown are p-wave velocity and the low-velocity anomaly at the bottom of 14-27 is artificial.

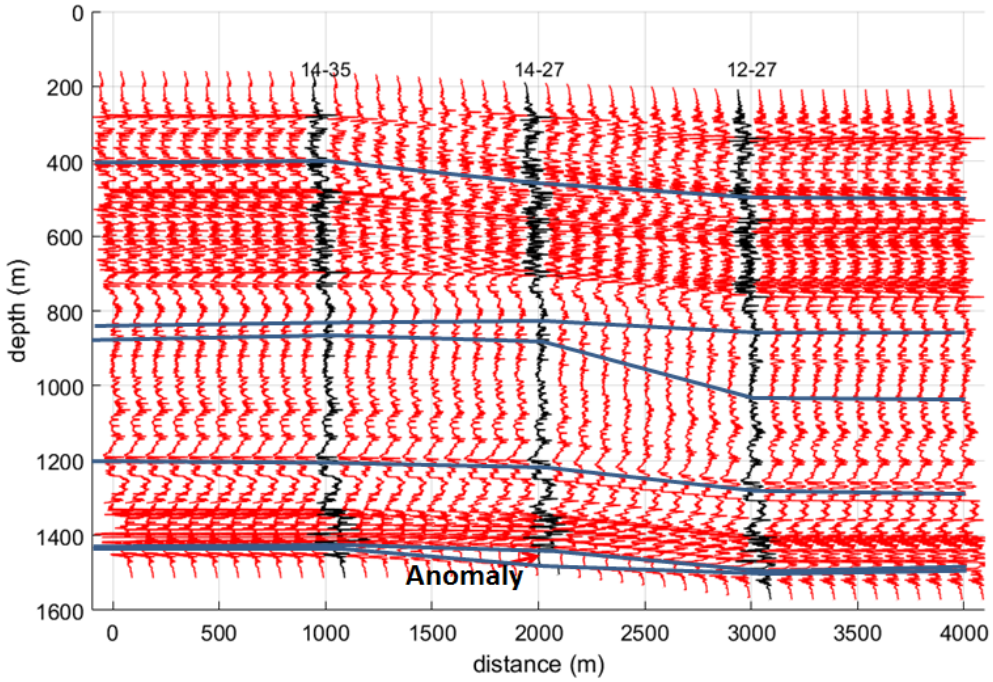

Figure 1: An illustration of a section of well logs that were spatially interpolated from three wells (black) available from the Hussar project. The interpolated logs (red) were interpolated along the formation tops (blue lines) with stretching or squeezing done to accommodate thicking or thinning of formations. The logs shown are p-wave velocity and the anomaly indicated on 14-27 was artificially introduced. The structure shown on the right-hand-side is mostly a reflection of a topographic high at well 12-27 that was not modelled.

In Figure 1, interpolated logs are shown every 100m but to create the data used here, interpolated logs were created every 2.5m. The vertical sampling of the interpolated logs was 0.5m so after interpolation the logs were downsampled using Backus averaging to create a section of well-log velocity values sampled on a 2.5m square grid. For the overburden (the upper 200m) a linear gradient was attached that trended from the value at the log top to a value of 1000m/s at the surface. Since the value at log top changes for each interpolated log, this resulted in lateral and vertical gradients in the overburden. Similarly, for the underburden (from log bottom to 2000m depth) a linear gradient was attached that trended from the value at log bottom to 4500m/s at 2000m depth. The resulting model is shown in Figure 2. Also shown in Figure 3 is the normal incidence reflectivity section computed from the velocity model and displayed in time. This is used in exploding reflector modelling.

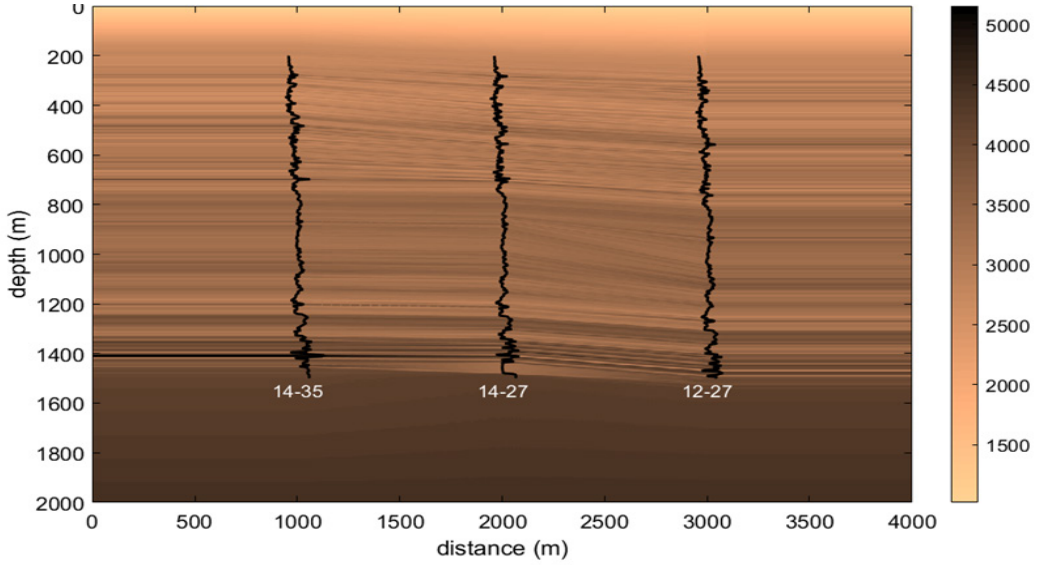

Figure 2: The interpolated velocity log section created for this study. Velocity logs were created every 2.5m (distance) and are sampled every 2.5m (depth). Colors indicate velocity in m/s. Considerable stratigraphic detail has been preserved and not the low velocity anomaly at the bottom of well 14-27.

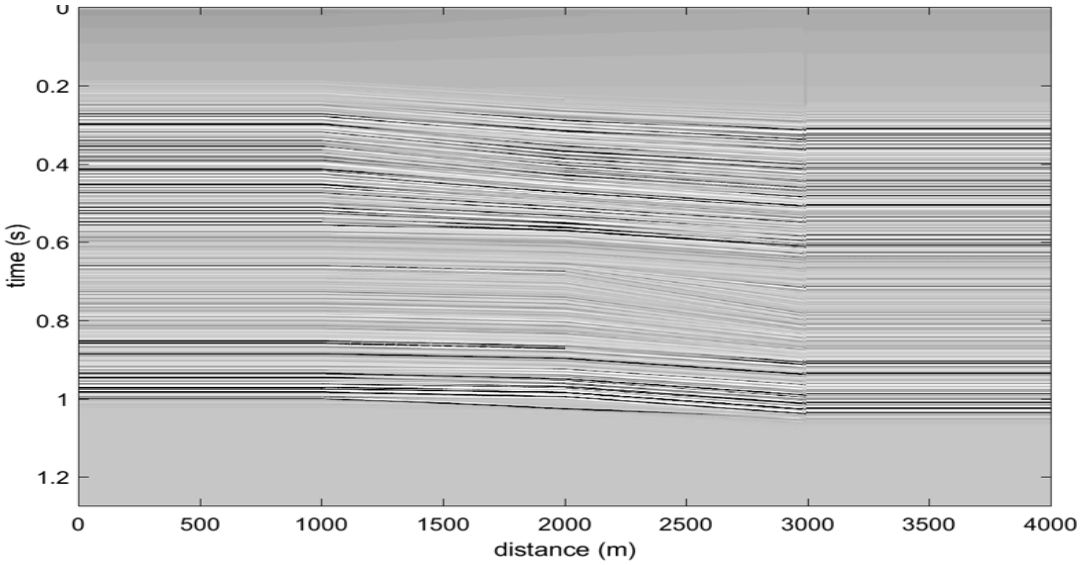

Figure 4: The reflectivity section computed from the velocity model of Figure 3. The section is displayed in time not depth and the apparent traveltime glitch at distance of 3000m is caused by an interpolation irregularity in the overburden.

Using the finite-difference modelling software in the CREWES Matlab toolbox (specifically *afd_shotrec_alt*), a set of 61 shot records were created with source positions at regular intervals along the distance axis. The source spacing is 66.7m, the receiver spacing is 2.5m, the time step size is 0.00025s, and the output time sample interval is 0.002s. The source wavelet had a dominant frequency of 50Hz and was minimum phase. An example of one of the shot records is shown in Figure 5. Immediately apparent is the very strong coherent noise that is associated with the free surface. While not a Rayleigh wave (elastic modelling is required for that) this noise plays a similar role in that it interferes with our ability to work with the underlying reflection data. Fortunately, as can

be seen in Figure 5, the source noise is well separated from the reflection data in the (k_x, f) domain and can be removed with an f-k fan filter.

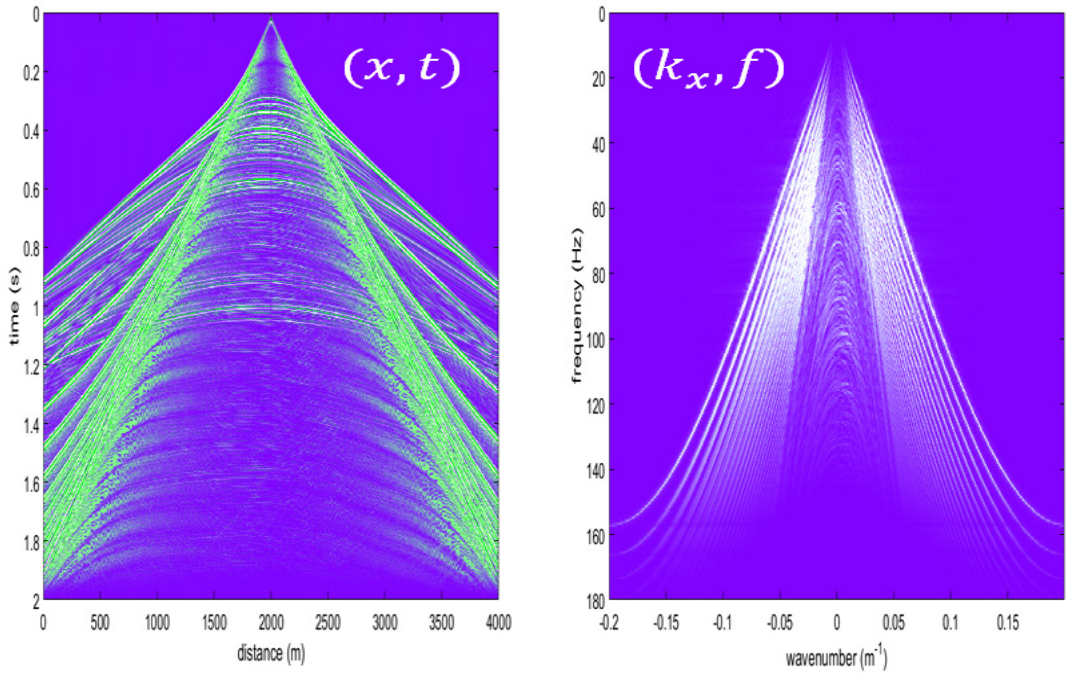

Figure 5: The center shot form the set of 61 that were created using the model of Figure 3 with the acoustic finite difference tools in the CREWES Matlab library. On the left is the shot in the (x, t) domain while on the right is the (k_x, f) domain.

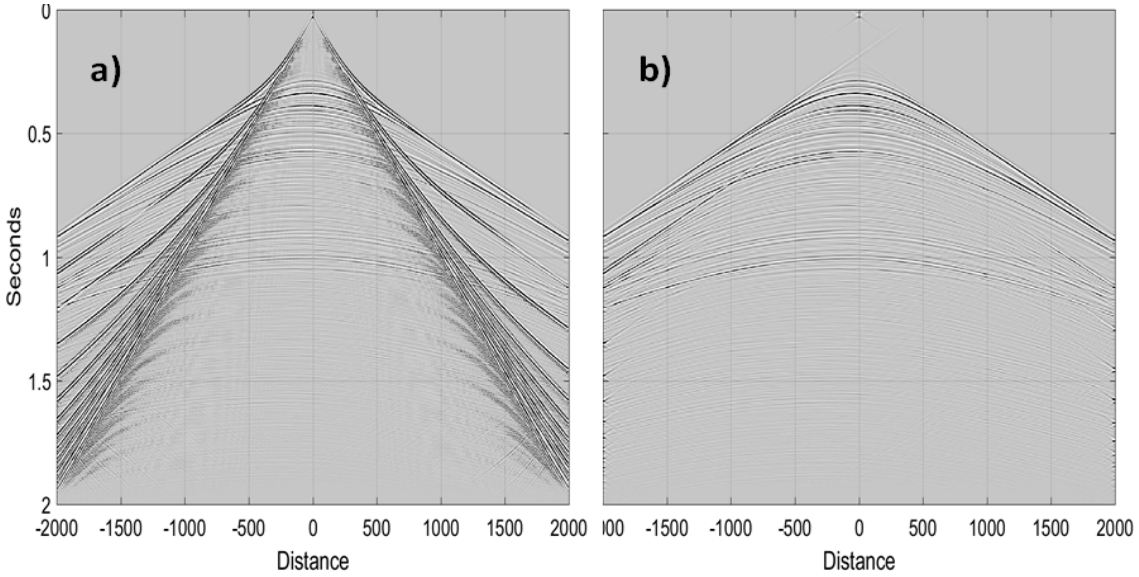

Figure 6: a) The shot record of Figure 5 before f-k fan filtering and b) after f-k fan filtering. The coherent noise from the source and associated with the free surface has been almost entirely removed.

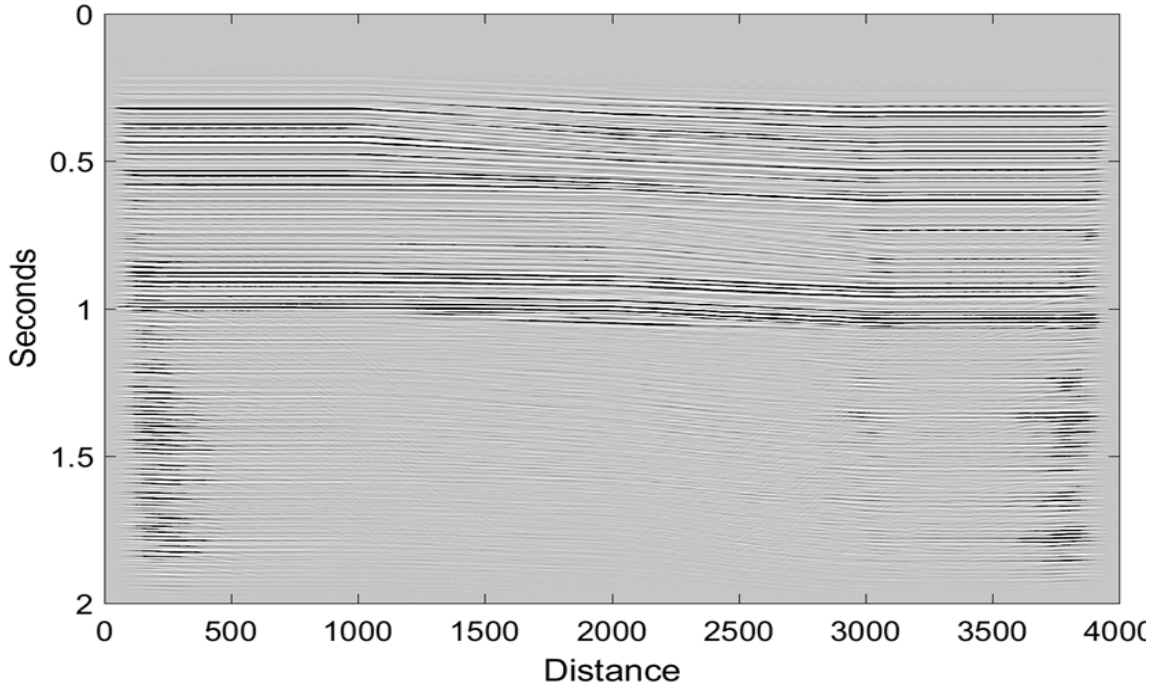

Figure 7: The CMP stack resulting from processing the 61 shot records simulated from the model of Figure 2. Compare with Figure 8.

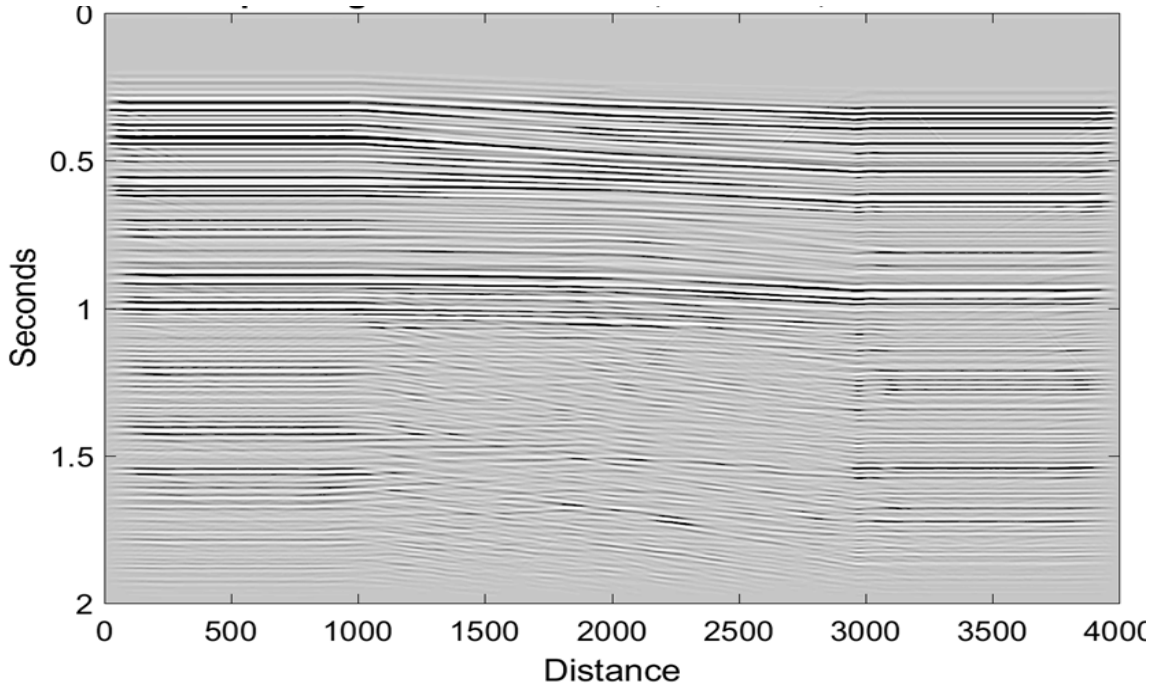

Figure 8: An exploding reflector simulation from the velocity model of Figure 2. Compared with the CMP stack in Figure 7, note the overall lower bandwidth and higher multiple content of the exploding reflector section. Every event below about 1.1 seconds is a multiple.

After f-k filtering, gain recovery, and normal moveout removal (using the exact RMS velocity model) the 61 shot records were stacked to produce the result shown in Figure 7. The very course shot spacing (66.7M) compared to the receiver spacing (2.5m) resulted in some footprint and this was suppressed using a time-variant trace mix that was 21

traces wide at 0.2s and 5 traces wide at 0.9s. Figure 8 shows a corresponding exploding reflector section. This was created using *afd_explode*. The finite-difference time stepping engine was identical for the shot records and the exploding reflector section and is second order in time and fourth order in space. However, the source function for the exploding reflector section is the reflectivity of Figure 4 but in depth and the velocities are all halved to get the same traveltimes as the CMP stack. Comparing Figures 7 and 8 shows two main differences between the sections. First, the exploding reflector section have much stronger multiples because the CMP stack has suppressed them. Second, the bandwidth of the exploding reflector section is lower than the stack even though the same wavelet was used. The reason for the second difference is not currently known.

Despite the differences in the two sections of Figures 7 and 8, it is still possible to consider the exploding reflector section as a simulation of the stack if these differences can be accounted for with simple processing. In the IMMI process, it is assumed that a well log is available at one or more locations. Choosing the location x=800m as the simulated well, we assume the reflectivity is known at this position from 200m depth to 1550m depth. This allows a primaries-only synthetic seismogram to be constructed at this location using a 40Hz zero phase wavelet. Then minimum-phase least-squares match filters can be determined at the well location to match each section to the synthetic seismogram. These filters where chosen to be 0.2s long and ones determine were applied to the entire section. Figure 9 shows the resulting well tie of both the CMP stack and the exploding reflector section and it is apparent that both tie very well, although the stack ties slightly better. This gives confidence that the stack can be simulated in a post-stack IMMI process using the exploding reflector model provided that both are tied to the well.

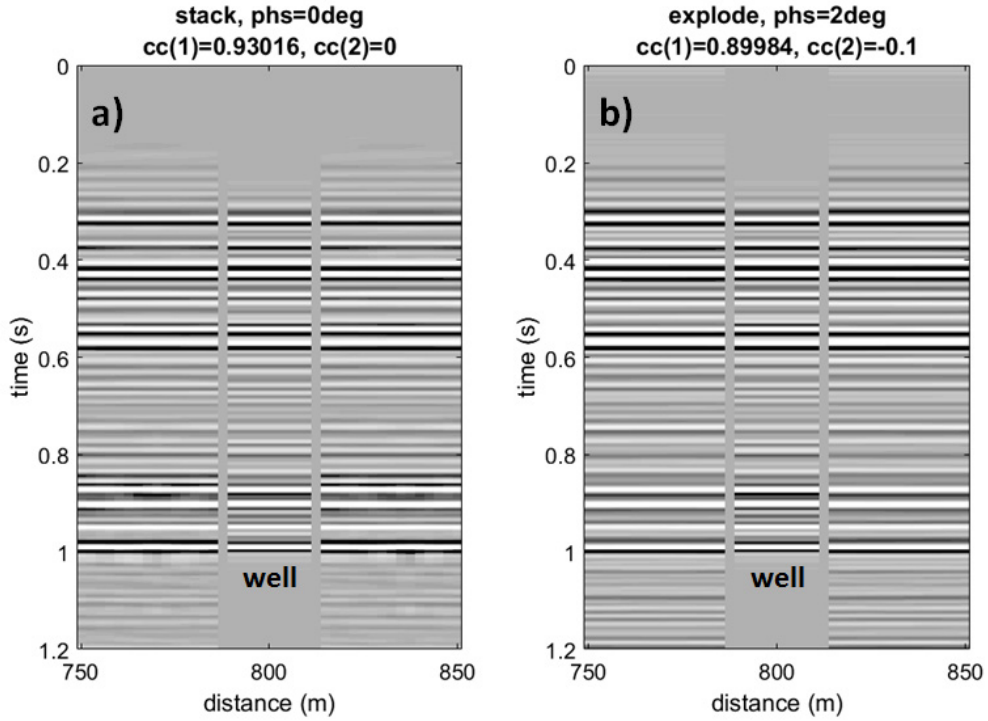

Figure 9: a) A portion of the stacked section after being match filtered to a synthetic seismogram created at the well which is at 800m. b) A portion of the exploding reflector section after being match filtered to the same synthetic seismogram. In both panels the traces marked 'well' are the

synthetic seismogram and are identical. The numbers annotated above the panels are (cc(1)) the maximum crosscorrelation of the panel with the well, and (cc(2)) the lag at which this maximum occurs. Also annotated is the apparent constant phase rotation between the panel and the seismogram.

POST-STACK IMMI

The process examined here consists first of creating an initial velocity model and simulating the exploding reflector response of this model. Then after creating a synthetic seismogram at the well, the seismogram and the two sections (stack and exploding reflector) are all send through the same bandpass filter to select the frequency band of emphasis in this iteration. Following Pratt (1999), the lowest frequencies are migrated first and the higher frequencies are gradually included as the iteration proceeds. To form the data residual, the two filtered sections are first matched to the filtered seismogram and then subtracted. The result is passed into PSPI (phase shift plus interpolation, Gazdag and Squazzero 1984) depth migration to create the estimated gradient. Finally the gradient is matched to the velocity in the well using either process of equation 3 or equation 7. Since the estimated gradient is a reflectivity estimate, we expect better performance from equation 7. This process is illustrated in Figure 10.

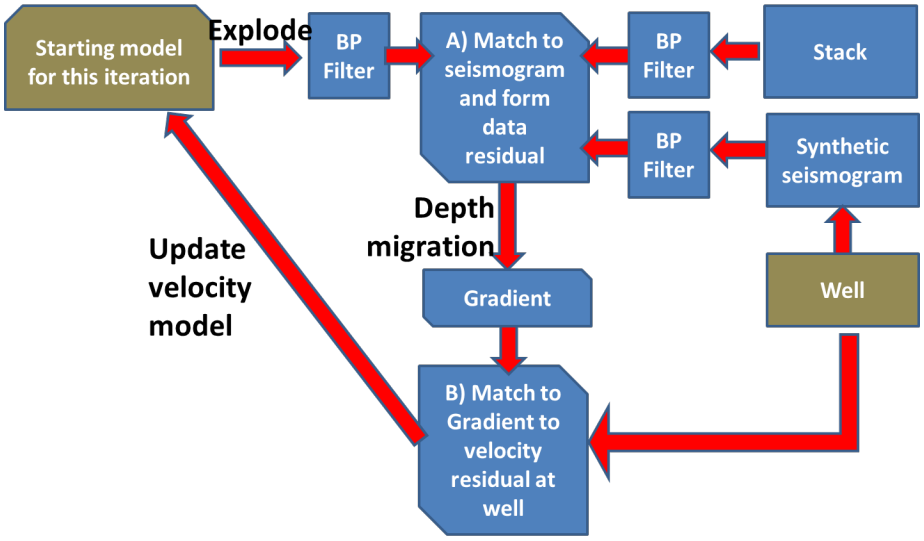

Figure 10: The post-stack IMMI process as implemented in this paper is illustrated for a single iteration. Two matching processes are involved: first in the time domain at A) the exploding reflector section and the stack are both matched to the synthetic seismogram, and second in the depth domain at B) the gradient (migrated data residual) is matched to the velocity residual at the well. Well information (brown) is used in both matching processes and in creating the starting model.

Figure 10 depicts a single iteration and it is anticipated that each iteration may possibly use a different set of frequencies. Since the exploding reflector modelling is a time-domain finite difference process, it is the same cost regardless of the frequency band that will be emphasize. The frequencies are selected by a bandpass filter which is implemented as a zero phase Butterworth filter. The iteration involves 3 distinct seismic datasets, the stack, the exploding reflector section, and the synthetic seismogram at the well. All three are passed through the same filter. After filtering, the two seismic sections are matched (denoted by A in Figure 10) to the synthetic seismogram using a

least-squares match filter. This is essential to get a meaningful data residual by simple subtraction. The data residual is then depth migrated to estimate the gradient. Here a post-stack implementation of PSPI is chosen but any post-stack depth migration could be used.

The depth migration must then be converted to a velocity perturbation. Since this is a depth domain matching, a convolutional match filter might not be appropriate. Theory suggests a scaling using equation 3 or equation 7 should be sufficient but it was found that this resulted in very slow improvement. Analysis suggested that the prestack gain recovery was not sufficient and that there was a slight decay with depth of reflection strength that did not match the well. Therefore, a linear with depth gain was applied, before computation of the scalar a, and described by

$$s_g(z) = s(z)\left(\frac{z}{z_0}\right)^n \tag{9}$$

where $s(z)$ is the depth trace at the well, $s_g(z)$ is the gained trace, and z_0 is the mean depth of the logged interval (200m to 1550m), and the optimal value of n was determined by direct search over the range -1 to 2 in increments of 0.2. For each value of n, a scalar a was computed and the squared error, $\sum_z\left(as_g(z) - \Delta v_w(z)\right)^2$ if using equation 3 or $\sum_z\left(2as_g(z)v_n(z) - \Delta v_w(z)\right)^2$ if using equation 7, was also evaluated. In both of these expressions $\Delta v_w = v_w - v_n$ is the residual velocity at the well where v_w is the logged velocity in the well and v_n is the velocity model at the well for iteration n. The optimal n and a are then chosen at the minimum squared error. Once determined they are applied to all traces in the gradient.

In preparing the background model, the usual approach of smoothing the exact model with a convolutional smoother was avoided as impractical. Instead, it was assumed that the overburden (the upper 200m) could be deduced from tomographic analysis of the diving waves apparent in Figure 5 and so this was taken as given. Then a linear function of depth was prescribed that graded from the overburden value at 200m depth to 4500m/s at 2000m depth. Figure 11 compares this initial model to the actual velocities in the true model at the locations of the three original wells of Figure 1. Clearly this model has very little of stratigraphic information in it and could conceivably be deduced in practice.

Figures 12 and 13 show two initial inversion results using an IMMI iteration in which the frequency bandwidth was expanded from 0-10Hz in the first iteration to 0-15Hz in the second and so on incrementing the maximum frequency by 5 Hz each time until 0-60Hz was reached in the 11th iteration. This will be called an expanding bandwidth iteration. The difference between these Figures is that Figure 12 was created using the inversion condition of equation 7 while Figure 13 used that of equation 3. As expected, equation 7 gives a clearly superior result and equation 3 was not further investigated. Note that the velocity anomaly at x=2000 and z=1450 has not been clearly resolved although more shallow features have been.

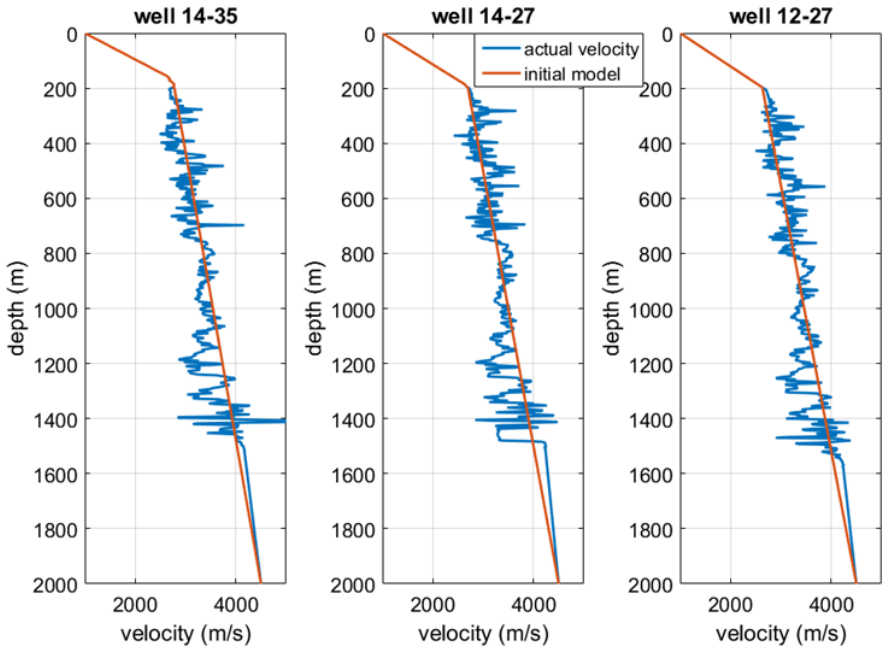

Figure 11: The initial model used the exact overburden (above 200m) and a simple linear trend from the base of the overburden to 4500m/s at 2000m depth. This figure shows how the initial model compares to the exact velocity at the 3 initial well locations of Figure 1.

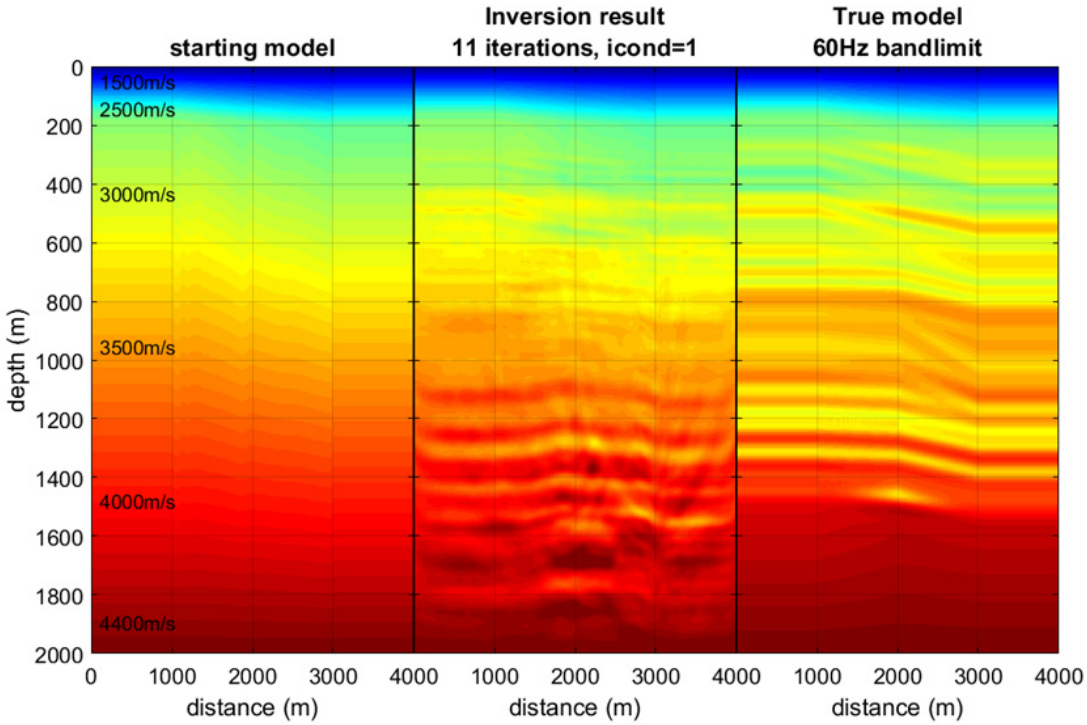

Figure 12: The result of an IMMI iteration using the inversion condition of equation 7 (called icond=1). There were 11 iterations during which the minimum frequency was always zero and the maximum frequency was 10, 15, 20, 25, 30, 35, 40, 45, 50, 55, 60 Hz. The correspondence between color and velocity in indicated on the left hand side of the starting model.

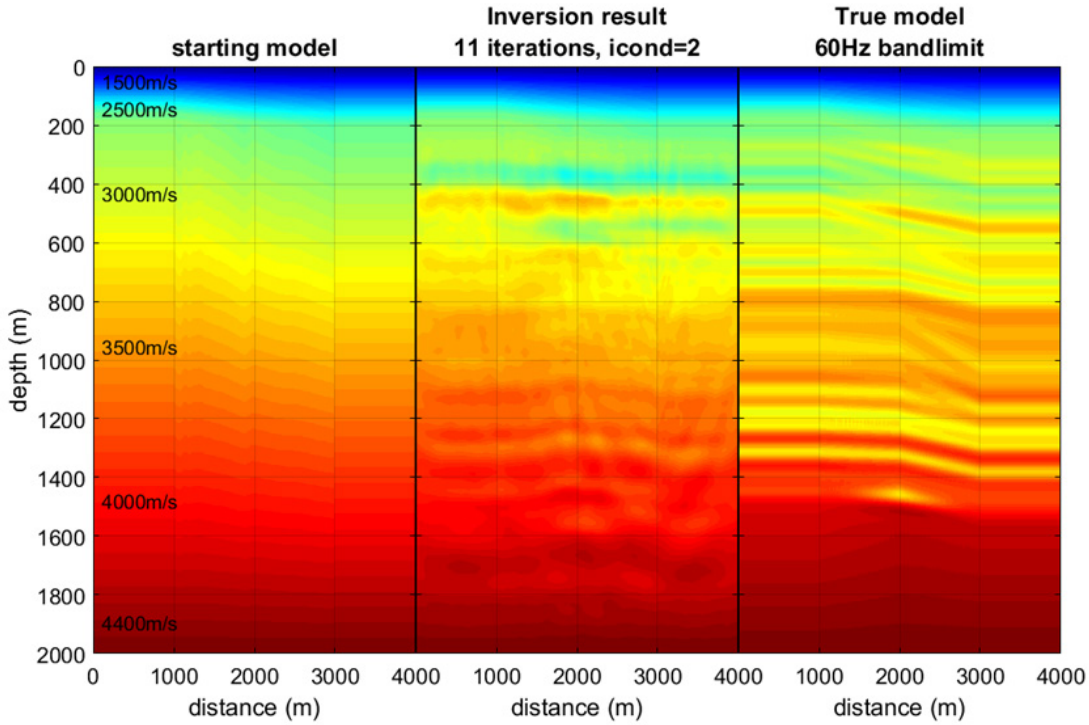

Figure 13: Similar to Figure 12 except that the inversion condition was that of equation 3 (denoted icond=2). Comparing to Figure 12, it is clear that this result has much less detail and is generally inferior.

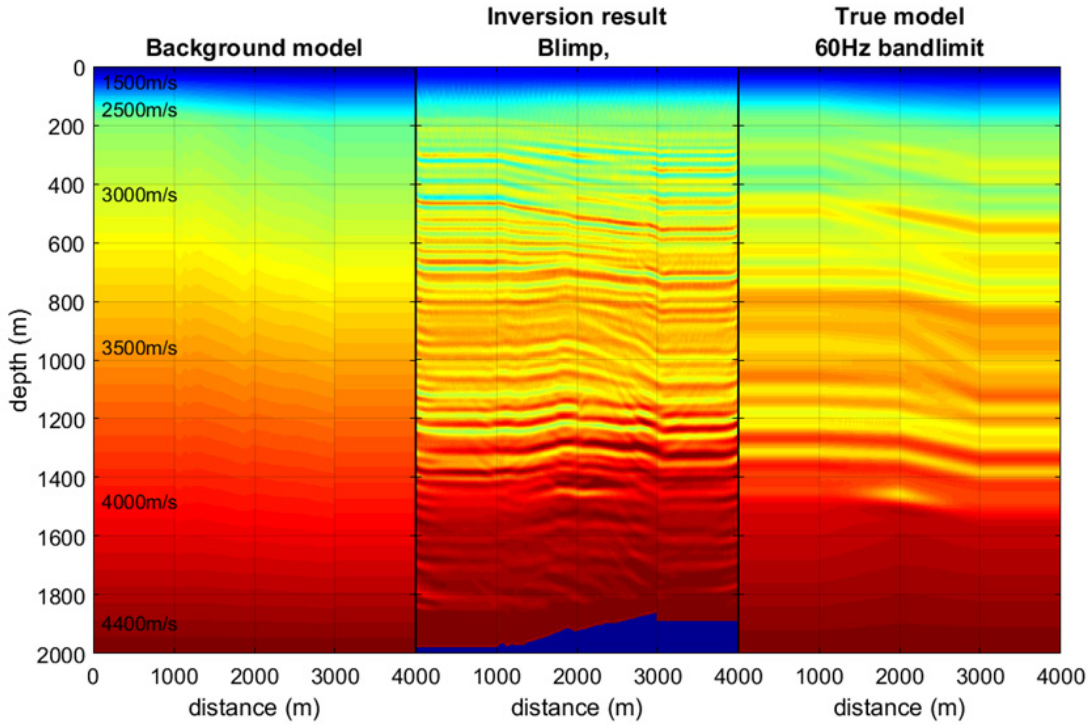

Figure 14: A conventional band-limited impedance inversion computed in time on a depth migrated section using the background model. The result is clearly different and more 'ringy' than that of Figure 12.

For comparison, Figure 14 shows a conventional band-limited impedance inversion of the stacked section. This was done by first depth migration the stack with the starting model, then converting to time and running impedance inversion using the CREWES *blimp* algorithm (Ferguson and Margrave, 1996), and then converting back to depth. While comparable to the result in Figure 12, it appears more 'ringy'. The velocity anomaly is resolved here more clearly than in Figure 12.

Many other frequency variations with iteration are possible and it is not clear what might be optimal. The result in Figure 12 is perhaps the best achieved so far. Figure 15 shows the result of 11 iterations of a 15Hz wide moving band. This means that each iteration used a 15Hz band width that began with 0-15Hz in iteration 1, moved to 5-20Hz in iteration 2, and finished at 50-65 Hz in iteration 11.

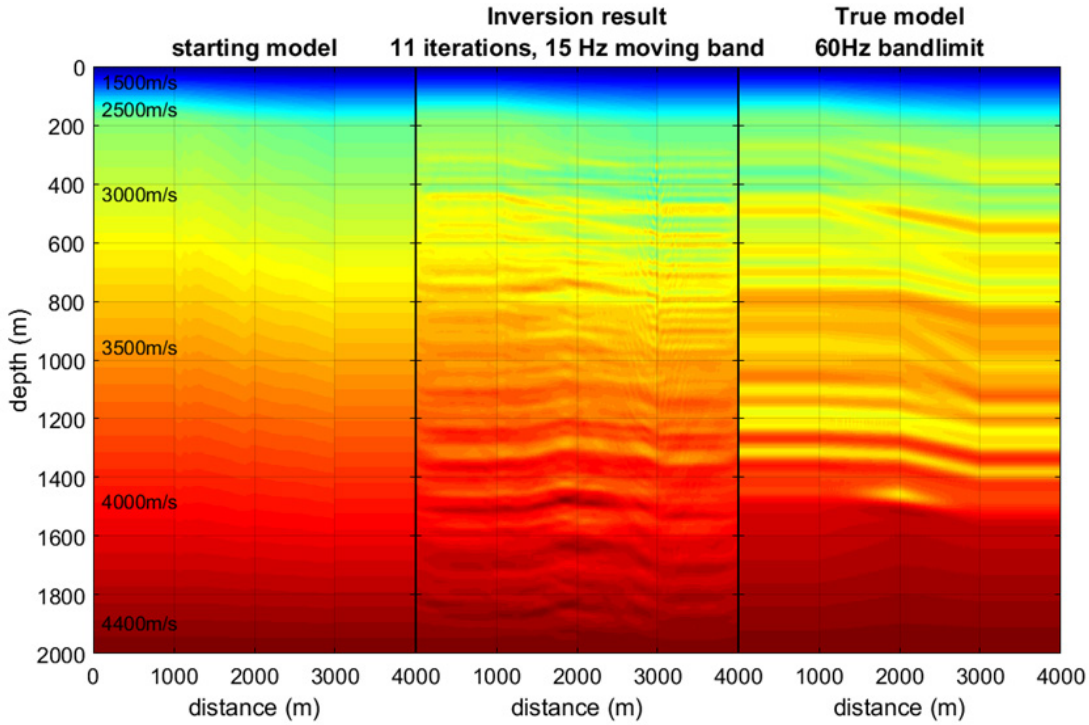

Figure 15: The result of 11 iterations using a 15 Hz wide moving frequency band. The first iteration used the 0-15Hz band, the second used 5-20Hz, and so on until the 11th used 50-65Hz. Compare with Figure 12.

Figures 16, 17, and 18 illustrate the convergence (or lack thereof) at three different locations: x=800, 2000, and 3000. The first location is that of the supposed well and the second is where the low velocity anomaly exists in the model. As these figures demonstrate convergence is best at the well and the latter half of the 11 iterations shows little change. Figure 19 shows 6 snapshots that are the velocity model at the end of every odd numbered iteration. Again it is apparent that there is little change after the 5th iteration. Moreover, it seems that the higher frequencies are having little effect on the result. This strongly suggests that there is much room for improvement in this process.

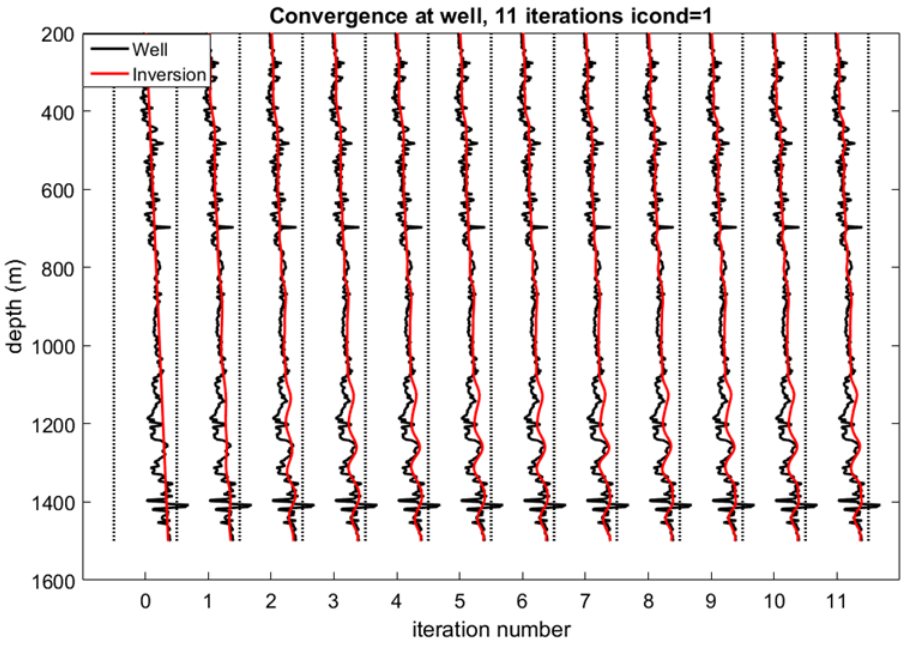

Figure 16: For the result of Figure 12, the convergence at the supposed well location (x=800m) is illustrated. It appears that these is very little evolution after iteration 5.

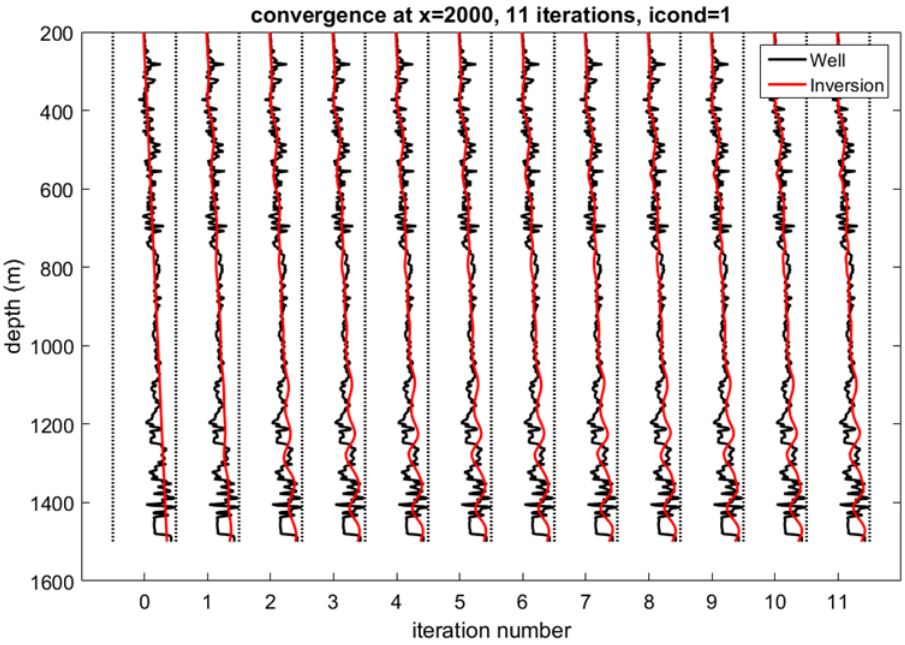

Figure 17: Similar to Figure 16 except for location x=2000m where there is a low velocity anomaly at z=1450m that is not resolved.

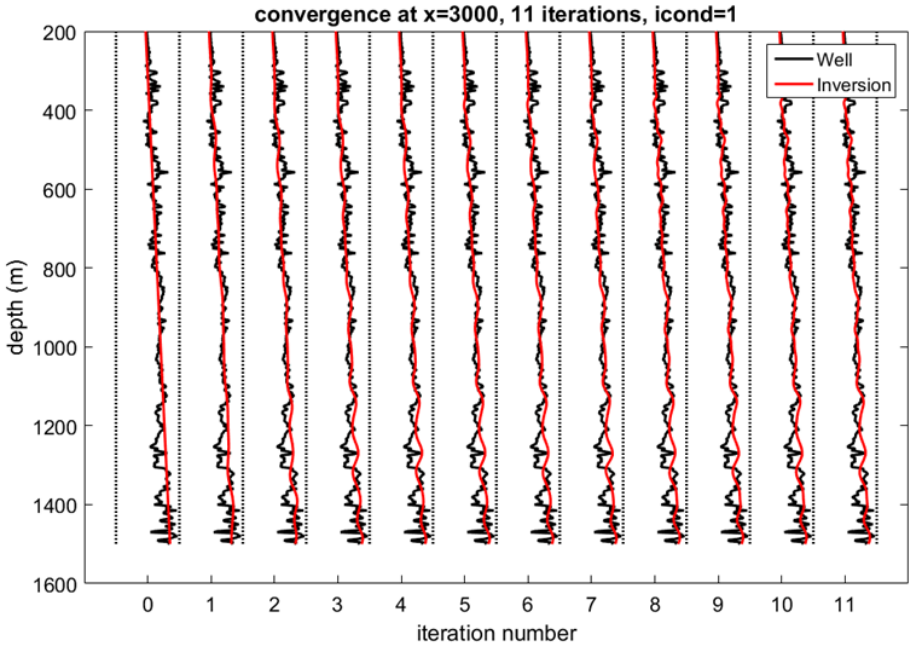

Figure 18: Similar to Figures 16 and 17 except for location x=300m.

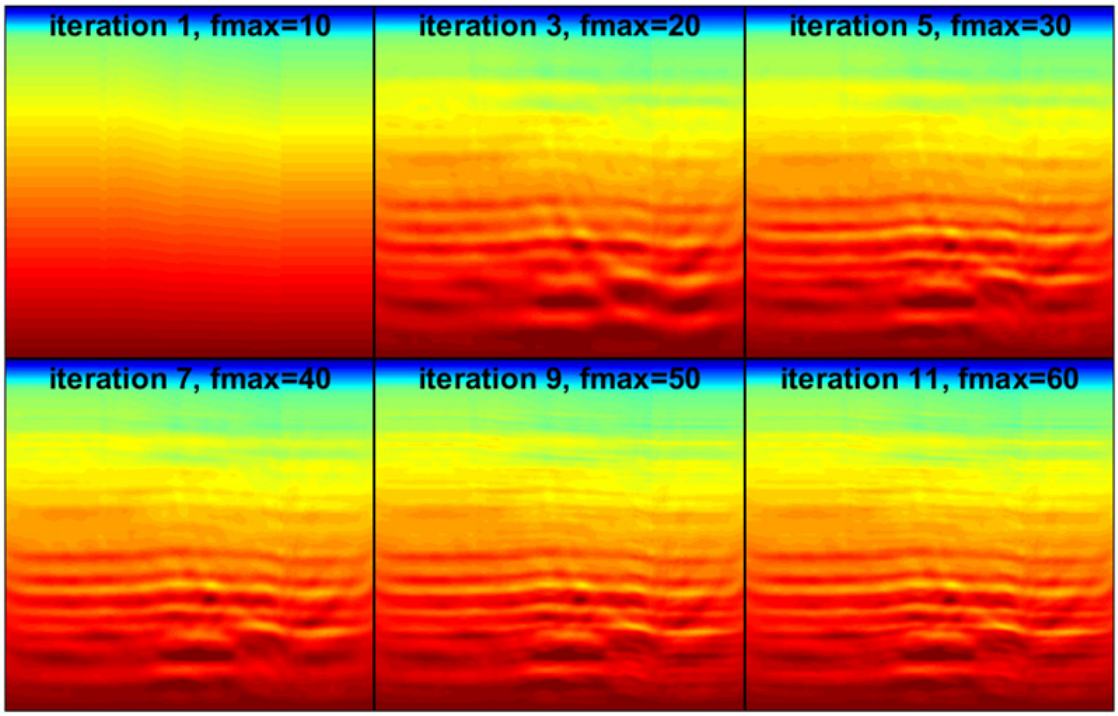

Figure 19: For the result of Figure 12, the evolution of the velocity model is illustrated. It is apparent that there is little change in the latter half of the iteration.

DISCUSSION AND CONCLUSIONS

It appears that a post-stack IMMI process is very possible and offers an interesting alternative to conventional impedance inversion. The stacked section can be effectively modelled by an exploding reflector algorithm. When one or more well logs are available they can be used to improve both the stack and the exploding reflector model by match filtering to a theoretical seismogram. The resulting data residual can then be depth migrated to compute an analog to the FWI gradient. Calibration of the gradient can be done using an impedance condition designed to convert reflectivity to an impedance perturbation. The resulting inversions show interesting features and details and are limited, in this case, by the nearly featureless starting model used. A more detailed starting model would produce better results. It also appears that the high frequencies are having little effect on the inversion and that the process described here could be greatly improved.

ACKNOWLEDGEMENTS

I thank the sponsors of the CREWES project for their support. This work was funded by CREWES industrial sponsors and NSERC (Natural Science and Engineering Research Council of Canada) through the grant CRDPJ 461179-13.

REFERENCES

Ferguson, R. J., and Margrave, G. F., 1996, A simple algorithm for band-limited impedance inversion: 8th Annual Research Report of the CREWES Project.

Gazdag, J., and Squazzero, P., 1984, Migration of seismic data by phase shift plus interpolation: Geophysics, **49**, 124-131.

Lailly, P., 1983, The seismic inverse problem as a sequence of before stack migrations: Conference on Inverse Scattering, Theory and Application, Society of Industrial and Applied Mathematics, Expanded Abstracts, 206-220.

Loewenthal, D., Lu, L., Roberson R., and Sherwood J., 1976, The wave equation applied to migration: Geophys. Prosp., 24, 380-399.

Margrave, G. F., Mewhort, L., Phillips, T, Hall, M., Bertram, M. B., Lawton, D. C., Innanen, K., Hall, K. W., and Bertram. K., 2011, The Hussar Low-Frequency Experiment: in the 23rd Annual Research Report of the CREWES Project.

Margrave, G. F., K. Innanen, and M. Yedlin, 2012, A Perspective on Full-Waveform Inversion: in the 24th Annual Research Report of the CREWES Project.

Pratt, R. G., 1999, Seismic waveform inversion in the frequency domain, Part I: Theory and verification in a physical scale model: Geophysics, 64, 888-901.

Shin, C., K. Yoon, K. J. Marfurt, K. Park, D.Yang, H. Y. Lim, S. Chung, and S. Shin, 2001, Efficient calculation of a partial-derivative wavefield using reciprocity for seismic imaging and inversion, Geophysics, 66, 1856-1863.

Tarantola, A., 1984, Inversion of seismic reflection data in the acoustic approximation: Geophysics, 49, 1259-1256.

Virieux, J., and S. Operto, 2009, An overview of full-waveform inversion in exploration geophysics: Geophysics, 74, WCC1-WCC26.